

Contents lists available at [ScienceDirect](https://www.sciencedirect.com)

## Journal of Biomechanics

journal homepage: [www.elsevier.com/locate/jbiomech](http://www.elsevier.com/locate/jbiomech)  
[www.JBiomech.com](http://www.JBiomech.com)

## Integrated iterative musculoskeletal modeling predicts bone morphology following brachial plexus birth injury (BPBI)

Nikhil N. Dixit<sup>a</sup>, Daniel C. McFarland<sup>a</sup>, Matthew B. Fisher<sup>a,b</sup>, Jacqueline H. Cole<sup>a,b</sup>, Katherine R. Saul<sup>a,\*</sup><sup>a</sup> North Carolina State University, Raleigh, NC, United States<sup>b</sup> University of North Carolina, Chapel Hill, NC, United States

## ARTICLE INFO

## Article history:

Accepted 21 January 2020

## Keywords:

Brachial plexus birth injury  
Preganglionic  
Postganglionic  
Finite element  
Computational model  
Bone growth  
Musculoskeletal

## ABSTRACT

Brachial plexus birth injury (BPBI) is the most common nerve injury among children. The glenohumeral joint of affected children can undergo severe osseous deformation and altered muscle properties, depending on location of the injury relative to the dorsal root ganglion (preganglionic or postganglionic). Preganglionic injury results in lower muscle mass and shorter optimal muscle length compared to postganglionic injury. We investigated whether these changes to muscle properties over time following BPBI provide a mechanically-driven explanation for observed differences in bone deformity between preganglionic and postganglionic BPBI. We developed a computational framework integrating musculoskeletal modeling to represent muscle changes over time and finite element modeling to simulate bone growth in response to mechanical and biological stimuli. The simulations predicted that the net glenohumeral joint loads in the postganglionic injury case were nearly 10.5% greater than in preganglionic. Predicted bone deformations were more severe in the postganglionic case, with the glenoid more declined (pre:  $-43.8^\circ$ , post:  $-51.0^\circ$ ), flatter with higher radius of curvature (pre: 3.0 mm, post: 3.7 mm), and anteverted (pre:  $2.53^\circ$ , post:  $4.93^\circ$ ) than in the preganglionic case. These simulated glenoid deformations were consistent with previous experimental studies. Thus, we concluded that the differences in muscle mass and length between the preganglionic and postganglionic injuries are critical mechanical drivers of the altered glenohumeral joint shape.

© 2020 Elsevier Ltd. All rights reserved.

## 1. Introduction

Brachial plexus birth injury (BPBI) is the most common nerve injury among children (Foad et al., 2008), caused by infant neck hyperextension during childbirth. The C5-C6 brachial plexus nerve roots are most commonly affected (Lagerkvist et al., 2010), leading to shoulder and elbow paralysis (Pearl, 2009). While many affected children spontaneously recover nerve and muscle function, 20% to 30% do not have total neurological recovery (Pondaag et al., 2004). Up to 33% of children affected with BPBI sustain permanent postural and bone deformities (Pearl, 2009), greatly impairing quality of life (Bae et al., 2008). Postural deformities include shoulder internal rotation and elbow flexion contractures (Waters, 2005). Concomitant altered upper limb bone growth can include retroversion, declination, and flattening of the glenoid fossa (Sibinski et al., 2010; Eismann et al., 2016), associated with partial humeral dislocation and severe shoulder instability (Kambhampati

et al., 2006; Di Mascio et al., 2011). Joint contractures, or restricted range of joint motion, are significantly correlated with glenohumeral bone deformities (Pearl and Edgerton, 1998; Kozin, 2004; Bhardwaj et al., 2013). Importantly, presentation in patients depends in part on nerve injury location relative to the nerve root ganglion. More severe contractures and bone deformity present for nerve root ruptures distal to the ganglion (postganglionic) (Waters, 2005), in contrast to avulsions proximal to the ganglion (preganglionic), which typically result in paralysis without shoulder or elbow contractures or significant bone deformity (Al-Qattan, 2003).

Understanding timing and mechanism of deformity initiation is essential for developing treatments to prevent bone and postural deformities from developing, rather than correcting deformity after formation. Because almost nothing is known about how bone tissue deformity first initiates, there is currently no consensus on optimal timing or treatment type (nerve repair or other therapy) post-injury (Belzberg et al., 2004; Hale et al., 2010), leading to inconsistent clinical outcomes and poor quality of life for children and their families who suffer from lack of guidance on the best treatment plan (DeMatteo et al., 2014). Animal and computational

\* Corresponding author at: North Carolina State University, 1840 Entrepreneur Drive, Campus Box 7910, Raleigh, NC 27695-7910, United States.

E-mail address: [ksaul@ncsu.edu](mailto:ksaul@ncsu.edu) (K.R. Saul).

studies suggest that reduced longitudinal growth (resulting in shorter optimal muscle lengths) of paralyzed muscles crossing the shoulder may explain both contracture and bone morphological changes in postganglionic BPBI (Crouch et al., 2015; Crouch et al., 2014). It is well known that bone shape and density are driven by mechanical environment (Duncan and Turner, 1995), but there are other drivers of growth and development which could be negatively affected by either disuse or direct nerve injury to bone following BPBI. Shorter optimal muscle lengths on the affected limb in rats and mice following postganglionic neurectomy (Nikolaou et al., 2011; Crouch et al., 2015) may be associated with higher passive muscle forces compared to a typically developing muscle in a given posture due to reduced excursion capacity, in the absence of other changes to muscle or tendon. Multibody dynamic simulations (Crouch et al., 2014; Cheng et al., 2015) suggest that reduced optimal muscle lengths are sufficient to lower external rotation range of motion and redirect glenohumeral joint reaction forces posteriorly. Our recent work using finite element analysis to predict glenoid morphology following BPBI suggests that declination and flattening of the glenoid fossa will be more severe under static joint loading with constant magnitude and direction of loading (as with paralysis) compared to dynamic loading; in a normal functioning shoulder both magnitude and direction of loading change as the humeral head rotates in the glenoid. Likewise, simulations predicted more severe declination and flattening with shorter optimal muscle lengths (as seen following both preganglionic and postganglionic BPBI) compared to normal muscle lengths (Dixit et al., 2019). This work suggests that both higher magnitude passive muscle forces and static joint reaction loads due to BPBI and its associated paralysis could cause glenohumeral morphological changes, in the absence of confounding factors such as changes to tendon length or stiffness or optimal muscle force associated with reduced muscle mass.

While there is no data indicating changes to tendon properties post brachial plexus injury, there is compelling evidence that muscle properties such as muscle mass and optimal muscle length differ between preganglionic and postganglionic injury, and these properties change over time during growth. Earlier work in mice suggested that longitudinal muscle growth is preserved after preganglionic injury, based on reduced joint contractures and retained ErbB signaling and spindle formation in biceps (Nikolaou et al., 2015). However, more recent work by our group characterized muscle architecture of all BPBI-affected shoulder muscles in a rat model of BPBI and revealed that optimal muscle lengths in affected muscles were, in fact, shorter after preganglionic injury compared to postganglionic injury (Dixit et al., 2020b). Notably, however, affected muscles in this preganglionic injury case also suffered markedly more muscle mass loss than after postganglionic injury (Crouch et al., 2015; Dixit et al., 2020b). Muscle mass and length are both related to muscle force production capacity (Zajac, 1989). Moreover, skeletal muscle is the fastest growing protein mass in neonates (Davis and Fiorotto, 2009), and growing skeletal size at this neonatal stage requires increasing muscle length in healthy development. Thus, this period of rapid musculoskeletal growth produces continual changes in the force production capacity of the muscles.

Therefore, the goal of this study was to evaluate whether changes to both muscle mass and optimal muscle length over time following BPBI provide a mechanically-driven explanation for the observed differences in bone deformity between preganglionic and postganglionic BPBI. We answered this question using a computational framework integrating musculoskeletal modeling to represent muscle changes over time and finite element modeling to simulate bone growth in response to mechanical and biological stimuli. Our hypothesis was that changes to muscle mass and optimal muscle length observed in preganglionic and post-

ganglionic BPBI are sufficient to account for glenohumeral bone deformities.

## 2. Methods

To evaluate effects of impaired longitudinal growth and muscle atrophy on bone growth over time, we implemented muscle architecture measured in a rat model of BPBI in an integrated iterative musculoskeletal modeling (I2M2) framework (Fig. 1). The approach incorporated muscle architectural properties, such as muscle length and muscle mass, as inputs to a multibody dynamic simulation (OpenSim 3.3, Stanford University) to predict shoulder joint reaction forces and apply these loads in finite element analysis (Abaqus 6.13.3, Dassault Systemes) to predict bone growth in response to biological and mechanical stimuli. To capture time-dependent changes inherent in a growing musculoskeletal system, at each time point, the new bone geometry was used to scale the musculoskeletal model and inform new joint reaction forces. These closed-loop simulations (MATLAB® R2016b, Mathworks) predict progression of joint deformation in response to changing joint loads over time. Specifically, we simulated bone growth under static postganglionic and preganglionic BPBI in a neonatal rat shoulder, for which quantitative descriptions of bone deformities are available for comparison (Li et al., 2010; Crouch et al., 2015). We simulated humeral head and scapular glenoid growth over 8 weeks of rat growth (equivalent to 2–7 human years) (Quinn, 2005) from a baseline undeformed initial condition representing 0 days postnatally. The initial geometry representing a neonatal stage for the simulation was obtained by isometrically reducing geometry obtained via micro-computed tomography (micro-CT) and corresponding muscle parameters in a typically developed 8-week-old rat to match bone lengths of a neonatal rat.

Multibody forward dynamic simulations of the glenohumeral joint were implemented in OpenSim 3.3 (Delp et al., 2007) using an existing musculoskeletal model of the shoulder as a foundation (Saul et al., 2015). Rat and human shoulder anatomy are known to be similar (Norlin et al., 1994), and the BPBI rat model has been shown to produce similar musculoskeletal changes as seen in human patients. The shoulder model was scaled using rat experimental data as described below. Twenty actuators representing muscles crossing the glenohumeral joint were included. We simulated denervation of muscles affected by C5-C6 level BPBI (deltoid, pectoralis major, biceps long head, biceps short head, subscapularis, supraspinatus, infraspinatus, teres major, and triceps long head) (Crouch et al., 2014; Cheng et al., 2015; Hogendoorn et al., 2010; Waters et al., 2009) by restricting activation level to 0 (passive contributions only), while unaffected muscles were activated at 30% (Waters et al., 2009). The muscle mass and optimal length (resting length) of affected muscles showing significant changes relative to the unaffected limb in both injury cases were obtained from our previous experiments in a rat model of BPBI (Dixit et al., 2020b). Spinal deltoid present in rats was incorporated in our musculoskeletal model in place of posterior deltoid muscle actuator due to anatomical similarity. Since these muscle changes were measured at 8 weeks of age in rats (Table 1), their effect was implemented in simulations by incrementing affected muscle PCSA and length linearly from 0 to 8 weeks over 15 simulation cycles to represent 8 weeks of musculoskeletal growth.

We assumed the ratio of muscle mass to optimal muscle length to be directly proportional to muscle physiological cross-sectional area (PCSA) for a given muscle, thereby affecting maximum isometric force development capacity. Similarly, changes to optimal muscle length for a given muscle were directly applied in the musculoskeletal model by reducing optimal muscle length by the % difference measured for affected muscles relative to the unimpaired

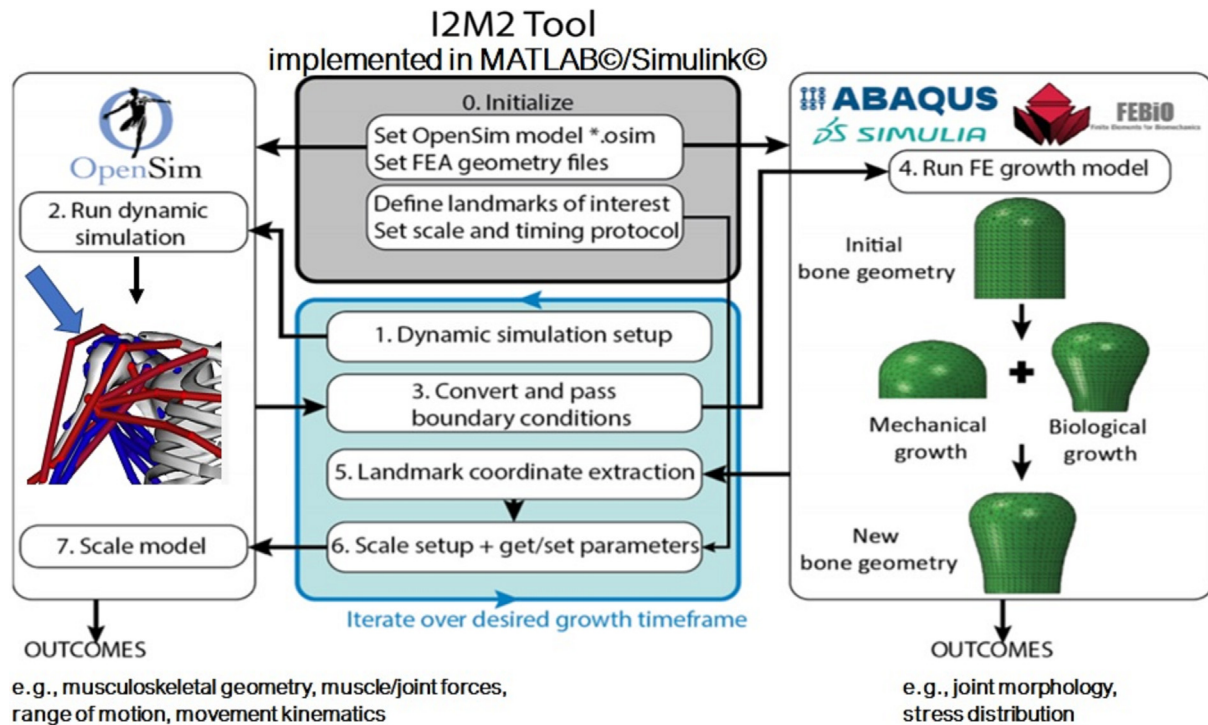


**Fig. 1.** Integrated iterative musculoskeletal modeling tool performs co-simulation between OpenSim and Abaqus. Forward dynamic simulations in OpenSim predict joint reaction forces, which are used by Abaqus as boundary conditions for bone growth computation. The changes to the bone shapes are communicated back to OpenSim such that it scales the musculoskeletal model for the next cycle of simulations.

**Table 1**

Experimentally determined changes in muscle mass and muscle length used as simulation inputs. No entry reflects no significant effect of BPBI injury case on this parameter for a given muscle.

Injury case	Metric (mean)	Deltoid	Spinal deltoid	Pectoralis major	Biceps long	Biceps short	Subscapularis	Supraspinatus	Infraspinatus	Teres major	Triceps long
Preganglionic	% muscle mass loss	71.0	64.6	-	76.8	-	70.0	83.6	78.8	54.5	23.5
	% restriction in optimal muscle length	-	22.3	-	22.3	20.0	-	32.4	-	29.3	-
Postganglionic	% muscle mass loss	38.0	41.5	25.3	54.3	-	24.0	-	-	36.9	42.1
	% restriction in optimal muscle length	-	14.5	11.2	-5.7	-	9.0	-	-	-	-

side (Table 1). We performed static studies at 30° abduction as a typical resting posture within the achievable range of motion for both injuries (Crouch et al., 2015, Dixit et al., 2019). Joint loads were computed at this posture and scaled using a force reduction factor based on a ratio of average PCSA of subscapularis and infraspinatus in neonatal rats to humans (Swan et al., 2014; Crouch et al., 2014). Force direction and magnitude calculated in simulations were applied as displacements in the finite element growth model. Our previous work describing simulations of glenohumeral joint growth using finite element analysis showed that the effective joint stiffness (applied reaction force/contact point displacement) during 8 weeks of bone development remains within 10% of the joint stiffness at the initial stage (Dixit et al., 2019). Therefore, resultant joint reaction forces were converted into corresponding displacements using a constant joint stiffness of 0.7 N/mm (Giorgi et al., 2014).

Joint loading boundary conditions were applied in an iterative finite element modeling approach (Dixit et al., 2019) to predict bone morphological growth in response to biological and mechanical stimuli. Initial geometry for all simulations was derived from an existing micro-CT scan of an uninjured neonatal rat (Crouch et al., 2015). The geometry was reduced to include only glenoid

and humeral head articulating surfaces to improve computational efficiency (Fig. 2). Because these neonatal bones are mostly cartilaginous in the region of interest, a cartilage material model was applied, with Young’s modulus of 1.1 MPa and Poisson’s ratio of 0.45 (Giorgi et al., 2014). We defined material properties to be

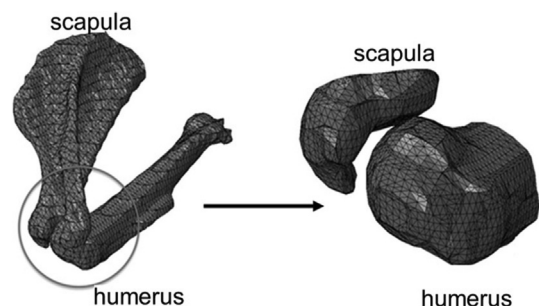


**Fig. 2.** Initial glenohumeral model geometry. Meshes defining the geometry of a typically developing neonatal rat scapula and humerus derived from microCT were reduced to include only the glenoid and humeral head articulating regions to increase computational efficiency.

linear elastic, isotropic, and homogenous. The geometry was meshed using quadratic tetrahedral elements (type C3D10M) with smaller elements near articulating surfaces. The final glenoid mesh contained 6,447 elements with 9,822 nodes, and humeral head mesh contained 4,730 elements with 7,109 nodes, based on a convergence study from our previous work (Dixit et al., 2019). A frictionless impenetrable surface-to-surface contact was defined between the articulating surfaces.

Biological growth was modeled as isometric, with constants applied such that the biological growth component was 75–85% of total growth (Germiller and Goldstein, 1997). Mechanical growth was proportional to compressive hydrostatic stress at every node. Stress due to static loads restricted growth (Giorgi et al., 2014):

$$\dot{\epsilon}_m = C_d \left( \frac{\sum_{i=1}^N \sigma_{hi}}{N} \right) \quad (1)$$

where  $\dot{\epsilon}_m$  is mechanical growth rate,  $\sigma_{hi}$  is compressive hydrostatic stress,  $N$  is number of movements per step, and  $C_d$  is chondrocyte density (Giorgi et al., 2014). Thermal expansion was used as an analog to incorporate deformations due to biological and mechanical growth. Growth rates determined from biological and mechanical governing equations were used to define temperature gradients to identify nodal deformations, and deformations were summed to create resultant deformed geometry.

After each cycle of finite element simulation, glenohumeral geometry was quantified by measuring in Abaqus nodal extrema along the three local coordinate axes of the glenoid and humeral

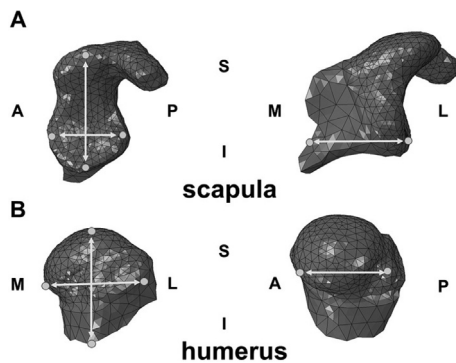


**Fig. 3.** The glenohumeral geometry after each cycle of finite element simulation was captured along the medial-lateral, superior-inferior, and anterior-posterior aspects of the (A) glenoid cavity and (B) humeral head by measuring specific nodal landmarks along the three anatomical axes. S – superior, I – inferior, A – anterior, P – posterior, M – medial, L – lateral.

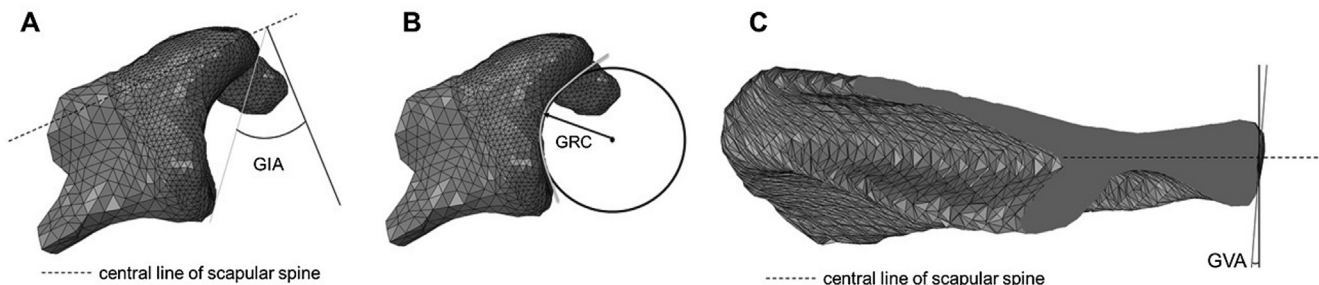


**Fig. 4.** Bone deformations were quantified by measuring A) glenoid inclination angle (GIA), B) glenoid radius of curvature (GRC), and C) glenoid version angle (GVA). GIA was defined in a local scapular plane, measured as the complementary angle to the angle between the scapular spine central line and the glenoid rim tangent. GRC was measured in the same scapular plane by fitting a circle to the glenoid curvature. GVA was defined in the transverse plane of the scapula in which the glenoid was widest, measured as the angle complementary to the angle between the plane of the scapular body and the tangent to the glenoid rim.

head (Fig. 3). New positions of nodal coordinates were stored and sent to a scaling algorithm in OpenSim, which scaled the musculoskeletal model according to distance between landmarks before and after a simulation cycle. Optimal length and mass of affected muscles were also updated in the scaled musculoskeletal model as described earlier for 1) preganglionic and 2) postganglionic cases (Table 1); muscles unaffected grew proportional to model scaling to represent normal growth. A forward dynamic simulation with the revised model was then performed to obtain new glenohumeral joint loads, and loads were used as a boundary condition for the next finite element iteration. In total, we performed 15 iterative growth cycles to simulate 8 weeks of postnatal growth.

Glenoid geometries for each simulation were assessed using glenoid inclination angle (GIA), glenoid radius of curvature (GRC), and glenoid version angle (GVA) after simulation cycles 0, 5, 10, and 15. GIA was defined in a local scapular plane, measured as the complementary angle to the angle between the scapular spine central line and glenoid rim tangent (Fig. 4A). GRC was measured in the same scapular plane by fitting a circle to glenoid curvature (Fig. 4B). GVA was defined in the scapular transverse plane in which the glenoid was widest, measured as the angle complementary to the angle between the scapular body plane and tangent to the glenoid rim (Fig. 4C). The GIA, GRC, and GVA predicted from I2M2 simulations were compared with existing geometry derived from micro-CT scans of rats at the same 8-week timepoint after preganglionic and postganglionic injuries (Dixit et al., 2020a). To evaluate the difference in the glenohumeral joint force production under simulated preganglionic and postganglionic injury cases, we used the joint force analysis tool in OpenSim to predict reaction loads at the glenohumeral interface.

### 3. Results

GIA at 8 weeks (15 simulation cycles) was more declined (uninjured GIA  $\sim -32.2 \pm 3.8^\circ$ ) (Dixit et al., 2020a) in the postganglionic case ( $-51.0^\circ$ ) compared to preganglionic case ( $-43.8^\circ$ ). Although both models started with identical geometries at the 1st cycle, GIA was predicted to be more declined (Fig. 5A and Fig. 6) in the postganglionic case for all the subsequent timepoints: 4.2% after 5 cycles, 5.8% after 10 cycles, and 16.4% after 15 cycles compared to the preganglionic case.

Simulations predicted higher GRC, or flatter glenoid, at 8 weeks (uninjured GRC  $\sim 44 \pm 1.5$  mm) (Dixit et al., 2020a) in the postganglionic injury simulation case (3.7 mm) than in the preganglionic case (3.0 mm). Simulations predicted a flatter glenoid in the postganglionic case by 20.0% after 5 cycles, 16.7% after 10 cycles, and 23.3% after 15 cycles compared to preganglionic case (Fig. 5B and Fig. 6). At 8 weeks, simulations predicted a more anteverted

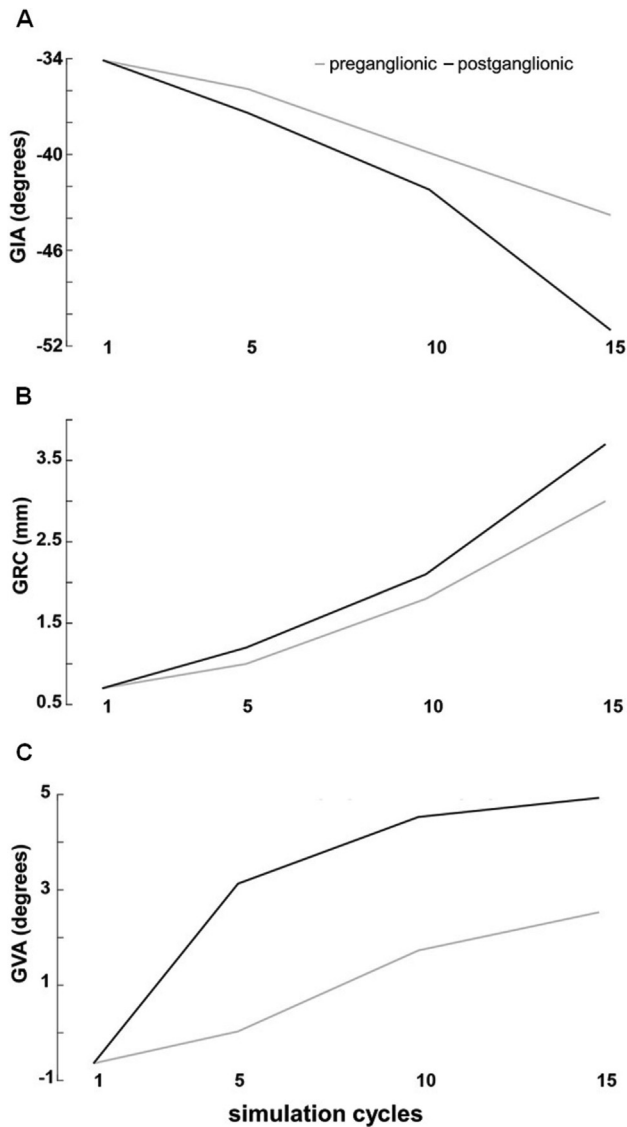


**Fig. 5.** Glenoid measurements after preganglionic and postganglionic injuries show change in A) GIA, B) GRC, and, C) GVA from 0 to 8 weeks of growth. The glenoid in the postganglionic case is more declined, flatter, and anteverted than in the preganglionic case.

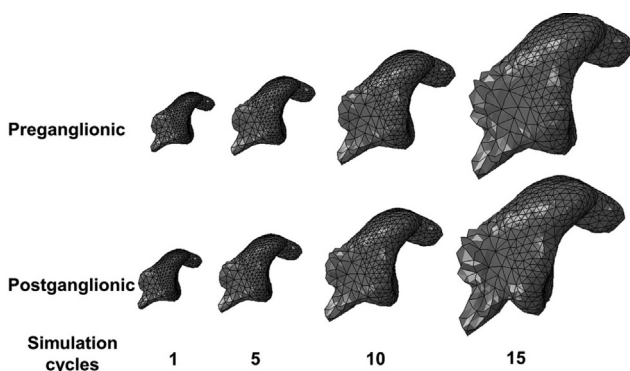


**Fig. 6.** Timeline of glenoid morphological changes over 8 weeks.

glenoid in the postganglionic case ( $5.0^\circ$ ) compared to the preganglionic case ( $2.5^\circ$ ) (uninjured  $GVA \sim 4.8 \pm 3.8^\circ$ ) (Dixit et al., 2020a) (Fig. 5C and Fig. 6).

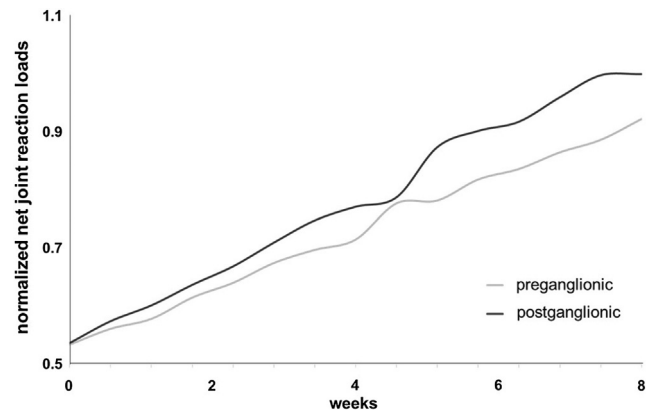


**Fig. 7.** Normalized net glenohumeral joint loads were lower in preganglionic case than the postganglionic injury cases over 15 simulation cycles representing 8 weeks of growth.

The net glenohumeral joint reaction forces in the postganglionic case were consistently higher at every timepoint than the preganglionic case. The net joint reaction forces in the postganglionic case were consistently higher by 4.4% after 5 cycles, 11.7% after 10 cycles, and 8.4% after 15 cycles than in the preganglionic case at same timepoint (Fig. 7).

#### 4. Discussion

We examined whether and to what extent changes in muscle mass and optimal muscle length following preganglionic and postganglionic BPBI influences postnatal glenohumeral joint morphogenesis, elucidating the mechanical factors responsible for joint deformity. Computational analyses predicted that net glenohumeral joint loading was higher in the postganglionic case than preganglionic and as a result there were more severe predicted bone deformations, suggesting that altered mechanical loading could account for observed changes in glenoid morphology after BPBI. Our past simulations (Crouch et al., 2014; Cheng et al., 2015) also revealed that these muscle changes could be drivers of increased postural deformity (i.e., contracture) in postganglionic but not preganglionic BPBI. Thus, taken together, these simulations reveal that mechanical underpinnings of both postural and bone deformity can be linked to altered structure of muscle. The current study also employed a new computational framework that integrated musculoskeletal dynamics with finite element simulations of growth to capture interactions of tissue growth and mechanical loading over time.

Joint reaction loads in both injury cases increased from 0 to 8 weeks, but at a slower rate in the preganglionic condition than in the postganglionic condition. Even though at every timepoint, preganglionic condition had shorter optimal muscle length (and were thus more stretched), muscle mass was also remarkably lower compared to muscles in the postganglionic condition at the same timepoint (Dixit et al., 2020b). The force developed by a muscle-tendon unit depends both on its length and cross-sectional area (Zajac, 1989). Shorter optimal muscle lengths will cause higher joint reaction forces (Cheng et al., 2015), especially the passive force component due to increased muscle stretch. However, lower muscle mass will substantially reduce passive force generation of affected muscles. The presence of joint contracture derives not from restricted longitudinal muscle growth alone but also depends on the extent to which muscle mass is lower following the injury (Dixit et al., 2020b). Thus, since joint loads were lower in the preganglionic case despite having shorter optimal muscle lengths compared to the postganglionic case, lower muscle

mass due to nerve injury appears to play a critical role, thereby contributing towards the reduction of overall joint load.

Prior work in rat BPBI models report glenoid deformities consistent with these simulations, including postganglionic deformities that are more severe than preganglionic, with higher declination (difference between injury cases =  $26.1 \pm 6.5^\circ$ ) and flatter radius of curvature (difference between injury cases =  $3.1 \pm 1.3$  mm) (Crouch et al., 2015; Dixit et al., 2020a). BPBI alters glenohumeral joint loads both in magnitude and in direction (Cheng et al., 2015). In addition, differences between injury cases for glenoid version were rarely significant and variable across studies whether postganglionic injury displayed retroversion ( $-0.9 \pm 3.7^\circ$ ) (Li et al., 2010) or anteversion ( $6 \pm 1.2^\circ$ ) (Li et al., 2008) relative to the unimpaired limb. In comparison, our simulations also predicted higher declination (more negative GIA) (difference =  $-7.2^\circ$ ) and more flatness (larger GRC) (difference = 0.7 mm), and minimal anteversion (more positive GVA) (difference =  $2.5^\circ$ ) in the postganglionic case. Differences were somewhat more remarkable in the experimental conditions on average, which may be attributable to limitations in the simulation conditions. Most notably, preganglionic injury did not exhibit contractures at the shoulder in our experimental studies (Dixit et al., 2020b) and some previous clinical work (Al-Qattan, 2003) but the postganglionic condition did, so a fully static shoulder in the preganglionic simulations is likely a conservative estimate of loading in this injury case.

This study provides a predictive framework for investigating effects of injury and therapy on altered bone development, which could assist clinicians in deciding timeline and targets for most effective intervention. Currently, even with surgical strategies such as external rotation tendon transfer (Eismann et al., 2016) or glenoid osteoplasty or osteotomy (Di Mascio et al., 2011), there is no consensus among surgeons as to whether deformities after BPBI are reversible after surgical intervention (Hogendoorn et al., 2010). This framework provides an opportunity to explore how bone deformation would progress over time. Similarly, it may provide guidance for intervention timing. For example, contracture and bone deformity was observed as early as 4-months old in human patients with postganglionic injuries, and less severe deformity in preganglionic injury (Al-Qattan, 2003). In simulation, GIA deforms at a higher rate in the postganglionic injury than in preganglionic injury, consistent with the clinical observation and suggesting a potentially more rapid rate of tissue change at odds with the wait-and-see approach currently used in clinical practice (Hale et al., 2010; Patra et al., 2016). Our simulations directly link changes in joint forces to altered shoulder morphology for BPBI. Thus, this work may support surgical or physical therapy interventions at an earlier time period that alters joint force direction and magnitude as a possible approach to limit progression of bone deformity.

The results of these computational simulations must be considered in light of the limitations. Muscle architecture following preganglionic and postganglionic BPBI were obtained at 8 weeks in rats (Dixit et al., 2020b). Although these muscle changes were implemented in simulations from 0 to 8 weeks through linear incrementation, only values for the 8-week time point have been measured; additional experimental data are needed to validate and refine at intermediate time points. Joint loading was obtained from a scaled musculoskeletal model using human glenohumeral joint as a foundation; while muscle and joint geometry and osseous morphological response to BPBI is very similar in rat and human shoulders (Norlin et al., 1994), they are not identical. There are limited data available describing operating ranges of shoulder muscles in rats or pediatric humans, but the limited data available (Crouch et al., 2015; Li et al., 2008; Li et al., 2010) suggests that rat anatomy is sufficiently similar for this study in which we are interested in how altered muscle mass and length in combination may

influence bone growth. For example, both rats and pediatric humans experience restrictions in external rotation range of motion and similar changes to glenoid geometry (Crouch et al., 2015; Cheng et al., 2015). Development of a rat forelimb musculoskeletal model should be pursued to improve representation of muscle and joint forces in future work. Joint stiffness, which was used to convert joint forces to equivalent displacements for application in finite element models, was constant in all simulations and over time. It is possible that effective stiffness may vary with condition or time; however, in our previous study (Dixit et al., 2019) joint stiffness under morphogenesis was found to be within 10% of the initial stiffness. Although cartilage is a biphasic material (Roddy et al., 2011), we modeled cartilage as a single-phase, nearly incompressible material (Poisson's ratio 0.49) (Giorgi et al., 2014). Previous studies (Carter and Wong, 2003; Shefelbine and Carter, 2004) have shown that the fluid pressure in biphasic models and hydrostatic stress in single phase models are similar when loaded at 1 Hz, which is approximately the frequency of muscle contraction (Vaal et al., 2000). In this study, static simulations did not have applied loading at 1 Hz. However, prior work in simulation of joint morphogenesis using a single-phase model were successfully extended to predict bone development under hip dysplasia under both static and dynamic loading (Giorgi et al., 2015; Giorgi et al., 2014). Additional future work is needed to capture effects of incorporating single-phase material in this framework when loading occurs under varied loading frequencies. Although we used a cartilaginous material model over the entire 8 weeks of growth simulation, some ossification occurs during this period; future simulations could incorporate evolving material models over time to address this limitation. The effect of synovial fluid at the joint does not play a crucial role in defining joint morphology (Giorgi et al., 2014); hence we did not model synovial fluid interface. We modeled isotropic biological growth for the glenoid, but there are multiple ossification centers at this stage of development (Nougarolis et al., 2017), and each may have different biological growth rates. We do not report changes to the humeral head; however, humeral head flatness has been reported in previous BPBI studies (Sibinski et al., 2010). To investigate the role of altered mechanical environment on bone growth, biological growth was held constant across all simulations, but the nerve injury may affect biological growth directly, and its effect on glenoid and humeral head shape should be investigated.

In conclusion, we found that changes to muscle mass and optimal muscle length over time due to BPBI are sufficient to explain key observed differences in bone and postural deformity between preganglionic and postganglionic BPBI. Using this computational framework, we predicted time progression of these osseous deformities and found that they are driven by altered joint reaction loads generated due to changes in muscle mass and optimal muscle length. The implementation of this framework is not limited to glenohumeral joint growth simulations due to BPBI, but can be used to predict growth for other joints following an injury or a disease.

## Acknowledgments

The research was funded by the National Center for Simulation in Rehabilitation Research (NIH P2CHD065690-06) and National Institutes of Health (NIH R21 HD088893). We have no conflicts of interest to report.

## References

- Al-Qattan, 2003. Obstetric brachial plexus palsy associated with breech delivery. *Ann. Plast. Surg.* 51, 257–264.

- Bae, D., Waters, P., Zurakowski, D., 2008. Correlation of pediatric outcomes data collection instrument with measures of active movement in children with brachial plexus birth palsy. *J. Pediatr. Orthopaed.* 28, 584–592 <http://ovidsp.ovid.com/ovidweb.cgi?T=JS&NEWS=n&CSC=Y&PAGE=fulltext&D=ovft&AN=01241398-200807000-00018>.
- Belzberg, A.J., Dorsi, M.J., Storm, P.B., Moriarity, J.L., 2004. Surgical repair of brachial plexus injury: a multinational survey of experienced peripheral nerve surgeons. *J. Neurosurgery* 101, 365–376 <https://www.ncbi.nlm.nih.gov/pubmed/15352592>.
- Bhardwaj, P., Burgess, T., Sabapathy, S.R., Venkataramani, H., Ilayaraja, V., 2013. Correlation between clinical findings and CT scan parameters for shoulder deformities in birth brachial plexus palsy. *The J. Hand Surgery* 38, 1557–1566 <http://www.ncbi.nlm.nih.gov/pubmed/23816519>.
- Carter, D., Wong, M., 2003. Modelling cartilage mechanobiology. *philosophical transactions of the Royal Society of London. Series B: Biolog. Sci.* 358, 1461–1471 <http://rsta.royalsocietypublishing.org/content/358/1437/1461.abstract>.
- Cheng, W., Cornwall, R., Crouch, D.L., Li, Z., Saul, K.R., 2015. Contributions of muscle imbalance and impaired growth to postural and osseous shoulder deformity following brachial plexus birth palsy: a computational simulation analysis. *J. Hand Surgery* 40, 1170–1176 <http://www.ncbi.nlm.nih.gov/pubmed/25847723>.
- Crouch, D.L., Hutchinson, I.D., Plate, J.F., Antoniono, J., Gong, H., Cao, G., Li, Z., Saul, K. R., 2015. Biomechanical basis of shoulder osseous deformity and contracture in a rat model of brachial plexus birth palsy. *the journal of bone and joint surgery. American Vol.* 97, 1264–1271 <http://www.ncbi.nlm.nih.gov/pubmed/26246261>.
- Crouch, D.L., Plate, J.F., Li, Z., Saul, K.R., 2014. Computational sensitivity analysis to identify muscles that can mechanically contribute to shoulder deformity following brachial plexus birth palsy. *J. Hand Surg* 39, 303–311 <http://www.ncbi.nlm.nih.gov/pubmed/24342260>.
- Davis, T., Fiorotto, M., 2009. Regulation of muscle growth in neonates. *Current Opin. Clin. Nutr. Metabolic Care* 12, 78–85 <http://ovidsp.ovid.com/ovidweb.cgi?T=JS&NEWS=n&CSC=Y&PAGE=fulltext&D=ovft&AN=00075197-200901000-00014>.
- Delp, S.L., Anderson, F.C., Arnold, A.S., Loan, P., Habib, A., John, C.T., Guendelman, E., Thelen, D.G., 2007. OpenSim: open-source software to create and analyze dynamic simulations of movement. *IEEE Trans. Biomed. Eng.* 54, 1940–1950 <http://ieeexplore.ieee.org/document/4352056>.
- DeMatteo, C., Bain, J.R., Gjertsen, D., Harper, J.A., 2014. 'Wondering and waiting' after obstetrical brachial plexus injury: Are we underestimating the effects of the traumatic experience on the families? *Plastic surgery. (Oakville, Ont.)* 22, 183–187.
- Di Mascio, L., Chin, K., Fox, M., Sinisi, M., 2011. Glenoplasty for complex shoulder subluxation and dislocation in children with obstetric brachial plexus palsy. *J. Bone Joint Surg. British Vol.* 93, 102–107 <http://www.ncbi.nlm.nih.gov/pubmed/21196552>.
- Dixit, N.N., McCormick, C.M., Cole, J.H., Saul, K.R., 2020a. Influence of brachial plexus injury location on morphology of the glenohumeral joint. *J. Hand Surg. (Submitted for publication)*
- Dixit, N.N., McCormick, C.M., Warren, E., Cole, J.H., Saul, K.R., 2020b. Preganglionic and postganglionic brachial plexus birth injury effects on shoulder muscle growth. *J. Hand Surg. (Submitted for publication)*
- Dixit, N.N., McFarland, D.C., Saul, K.R., 2019. Computational analysis of glenohumeral joint growth and morphology following a brachial plexus birth injury. *J. Biomech.* 86, 48–54 <https://www.sciencedirect.com/science/article/pii/S0021929019300776>.
- Duncan, R.L., Turner, C.H., 1995. Mechanotransduction and the functional response of bone to mechanical strain. *Calcif. Tissue Int.* 57, 344–358 <https://www.ncbi.nlm.nih.gov/pubmed/8564797>.
- Eismann, E.A., Laor, T., Cornwall, R., 2016. Three-dimensional magnetic resonance imaging of glenohumeral dysplasia in neonatal brachial plexus palsy. *J. Bone Joint Surg. American Vol.* 98, 142–151 <http://www.ncbi.nlm.nih.gov/pubmed/26791035>.
- Foad, S.L., Mehlman, C.T., Ying, J., 2008. The epidemiology of neonatal brachial plexus palsy in the United States. *J. Bone Joint Surg.* 90, 1258–1264 <http://jbjss.org/article.aspx?articleid=28711>.
- Germiller, J.A., Goldstein, S.A., 1997. Structure and function of embryonic growth plate in the absence of functioning skeletal muscle. *J. Orthopaedic Res. Off. Publicat. Orthopaed. Res. Soc.* 15, 362–370 <http://www.ncbi.nlm.nih.gov/pubmed/9246082>.
- Giorgi, M., Carriero, A., Shefelbine, S.J., Nowlan, N.C., 2015. Effects of normal and abnormal loading conditions on morphogenesis of the prenatal hip joint: application to hip dysplasia. *J. Biomech.* 48, 3390–3397 <http://www.sciencedirect.com/science/article/pii/S0021929015003395>.
- Giorgi, M., Carriero, A., Shefelbine, S.J., Nowlan, N.C., 2014. Mechanobiological simulations of prenatal joint morphogenesis. *J. Biomech.* 47, 989–995 <http://www.ncbi.nlm.nih.gov/pubmed/24529755>.
- Hale, H.B., Bae, D.S., Waters, P.M., 2010. Current concepts in the management of brachial Plexus Birth Palsy. *J. Hand Surg* 35, 322–331 <http://www.sciencedirect.com/science/article/pii/S0363502309010612>.
- Hogendoorn, S., Overvest, Van, Karlijn, L.J., Watt, I., Duijsens, A.H.B., Nelissen, Rob G H H., 2010. Structural changes in muscle and glenohumeral joint deformity in neonatal brachial Plexus Palsy. *J. Bone Joint Surg.* 92, 935–942 <http://jbjss.org/article.aspx?articleid=5973>.
- Kambhampati, S.B.S., Birch, R., Cobiella, C., Chen, L., 2006. Posterior subluxation and dislocation of the shoulder in obstetric brachial plexus palsy. *J. Bone Joint Surg. British Vol.* 88, 213–219 <http://www.ncbi.nlm.nih.gov/pubmed/16434527>.
- Kozin, S.H., 2004. Correlation between external rotation of the glenohumeral joint and deformity after brachial plexus birth palsy. *J. Pediatr. Orthop.* 24, 189–193 <http://japanknowledge.com/lib/display/?lid=40300SPED510400>.
- Lagerkvist, A., Johansson, U., Johansson, A., Bager, B., Uvebrant, P., 2010. Obstetric brachial plexus palsy: a prospective, population-based study of incidence, recovery, and residual impairment at 18 months of age. *Dev. Med. Child Neurol.* 52, 529 <http://www.ncbi.nlm.nih.gov/pubmed/20041937>.
- Li, Z., Barnwell, J., Tan, J., Koman, A.L., Smith, B.P., 2010. Microcomputed tomography characterization of shoulder osseous deformity after brachial plexus birth palsy: a rat model study. *J. Bone Joint Surg.* 92, 2583–2588 <http://jbjss.org/article.aspx?articleid=5797>.
- Li, Z., Ma, J., Apel, P., Carlson, C.S., Smith, T.L., Koman, L.A., 2008. Brachial plexus birth palsy-associated shoulder deformity: a rat model study. *J. Hand Surg.* 33, 308–312 <http://www.sciencedirect.com/science/article/pii/S0363502307010398>.
- Nikolaou, S., Hu, L., Cornwall, R., 2015. Afferent innervation, muscle spindles, and contractures following neonatal brachial plexus injury in a mouse model. *J. Hand Surg.* 40, 2007 <http://www.ncbi.nlm.nih.gov/pubmed/26319770>.
- Nikolaou, S., Peterson, E., Kim, A., Wylie, C., Cornwall, R., 2011. Impaired growth of denervated muscle contributes to contracture formation following neonatal brachial plexus injury. *J. Bone Joint Surg.* 93, 461–470 <http://jbjss.org/article.aspx?articleid=6228>.
- Norlin, R., Hoe-Hansen, C., Oquist, G., Hilderbrand, C., 1994. Shoulder region of the rat: anatomy and fiber composition of some suprascapular nerve branches. *Anatomical Record* 239, 332–342.
- Nougarolis, F., Mokrane, F., Sans, N., Rousseau, H., Dedouit, F., Telmon, N., 2017. Bone age estimation based on multislice computed tomography study of the scapula. *Int. J. Legal Med.* 131, 547–558 <https://search.proquest.com/docview/1867560323>.
- Patra, S., Narayana Kurup, J.K., Acharya, A.M., Bhat, A.K., 2016. Birth brachial plexus palsy: a race against time. *BMJ Case Rep.* 2016, bcr2016215996 <https://www.ncbi.nlm.nih.gov/pubmed/27402656>.
- Pearl, M.L., 2009. Shoulder problems in children with brachial plexus birth palsy: evaluation and management. *J. American Academy Orthopaed. Surg.* 17, 242 <http://www.jaao.org/content/17/4/242.abstract>.
- Pearl, M.L., Edgerton, B.W., 1998. Glenoid deformity secondary to brachial plexus birth palsy. *J. Bone Joint Surg.* 80, 659–667 <http://jbjss.org/article.aspx?articleid=24019>.
- Pondaag, W., Malessy, M.J., Gert van Dijk, J., Thomeer, R.T., 2004. Natural history of obstetric brachial plexus palsy: a systematic review. *Dev. Med. Child Neurol.* 46, 138–144 [http://journals.cambridge.org/abstract\\_S0012162204000258](http://journals.cambridge.org/abstract_S0012162204000258).
- Quinn, R., 2005. Comparing rat's to human's age: How old is my rat in people years? *Nutrition.* 21, 775–777 <https://www.sciencedirect.com/science/article/pii/S089900705001711>.
- Roddy, K.A., Kelly, G.M., van Es, M.H., Murphy, P., Prendergast, P.J., 2011. Dynamic patterns of mechanical stimulation co-localise with growth and cell proliferation during morphogenesis in the avian embryonic knee joint. *J. Biomech.* 44, 143–149 <http://www.sciencedirect.com/science/article/pii/S0021929010004860>.
- Shefelbine, S., Carter, D., 2004. Mechanobiological predictions of femoral anteversion in cerebral Palsy. *Ann. Biomed. Eng.* 32, 297–305 <http://www.ncbi.nlm.nih.gov/pubmed/15008378>.
- Sibinski, M., Woźniakowski, B., Drobniewski, M., Synder, M., 2010. Secondary glenohumeral joint dysplasia in children with persistent obstetric brachial plexus palsy. *Int. Orthop.* 34, 863–867 <http://www.ncbi.nlm.nih.gov/pubmed/20174796>.
- Swan, M.A., Sato, E., Galatz, L.M., Thomopoulos, S., Ward, S.R., 2014. The effect of age on rat rotator cuff muscle architecture. *J. Shoulder Elbow Surg/American Shoulder Elbow Surg. et al.* 23, 1786–1791 <http://www.ncbi.nlm.nih.gov/pubmed/24878035>.
- Vaal, J., van Soest, A.K., Hopkins, B., 2000. Spontaneous kicking behavior in infants: Age-related effects of unilateral weighting. *Development. Psychobiol.* 36, 111–122 [http://onlinelibrary.wiley.com/doi/10.1002/\(SICI\)1098-2302\(200003\)36:23.0.CO;2-H/abstract](http://onlinelibrary.wiley.com/doi/10.1002/(SICI)1098-2302(200003)36:23.0.CO;2-H/abstract).
- Waters, P., 2005. Update on management of pediatric brachial plexus palsy. *J. Pediatr. Orthopaed.* B. 14, 233–244 <http://ovidsp.ovid.com/ovidweb.cgi?T=JS&NEWS=n&CSC=Y&PAGE=fulltext&D=ovft&AN=01202412-200507000-00001>.
- Waters, P.M., Monica, J.T., Earp, B.E., Zurakowski, D., Bae, D.S., 2009. Correlation of radiographic muscle cross-sectional area with glenohumeral deformity in children with brachial plexus birth palsy. *J. Bone Joint Surg.* 91, 2367–2375 <http://jbjss.org/article.aspx?articleid=28958>.
- Zajac, F.E., 1989. Muscle and tendon: properties, models, scaling, and application to biomechanics and motor control. *Crit. Rev. Biomed. Eng.* 17, 359 <https://www.ncbi.nlm.nih.gov/pubmed/2676342>.